Turkish Journal of Electrical Engineering & Computer Sciences

http://journals.tubitak.gov.tr/elektrik/

Research Article

Turk J Elec Eng & Comp Sci
(2017) 25: 2308 – 2321

doi:10.3906/elk-1603-297

Planar array of right-angled isosceles triangular microstrip antenna using Koch and meander lines for the Internet of things

Manisha GUPTA[1], **Vinita MATHUR**[2,*]
[1]Department of Physics, JECRC University, Jaipur, India
[2]Department of Electronics and Communication, JECRC University, Jaipur, India

Received: 31.03.2016 • **Accepted/Published Online:** 01.09.2016 • **Final Version:** 29.05.2017

Abstract: An ultrawideband antenna array using a right-angled isosceles triangular microstrip antenna as a basic element is presented using inset feed for applications in the Internet of things. A Koch fractal antenna array with defected ground plane is used to generate multiband applications. Further, meander lines are added to increase the equivalent inductance that reduces the size of the antenna and increases the bandwidth and gain. Antenna arrays have been constructed and experimentally studied. The measured results show good agreement with the numerical prediction and wideband operation.

Key words: Right-angled isosceles triangle microstrip antenna, ultrawideband, planar array, inset feed, meander lines, Internet of things

1. Introduction

In wireless communication systems for the ultrawideband (UWB) range such as aircraft, spacecraft, satellite, missile, and mobile radio applications in which high performance is required, low-profile antennas are necessary for the exchange of information. Microstrip patch antennas are used to meet these requirements [1,2]. These antennas can be realized on printed-circuit technologies with relatively small substrate areas. The losses because of the transmission line, antenna, and standing waves are undesirable for better transmission. The standing waves can be reduced by matching the load of the antenna to the characteristic impedance of the line in order to achieve maximum power transfer. Various techniques have been used to achieve this matching by using substrate material that has a dielectric constant with high value, patches that have slots in them, fractals, defected ground structure, electronic band gap structures, metamaterials, and shorting pins and plates [3–7]. Apart from losses there are methods to improve the efficiency, bandwidth, and gain, which can be achieved by increasing the height of the dielectric substrate, decreasing the relative permittivity, and performing dual-band operations [8,9]. A fractal antenna is commonly used for multiband applications. Applications like miniaturization and ultraband techniques can be provided by fractal geometry in antenna design due to its properties like self-similar space filling [10,11]. Antenna radiation efficiency is thought to be improved by a large number of bends and corners in many such fractals. It was found that using fractal patches substantially decreases the mutual coupling between elements [12–14].

The behavior of radiating patches in transmission networks has been improved by using array antennas as it increases the efficiency [15–17]. Array performance is affected by fractal type, spacing between elements,

*Correspondence: vinitamathur12@gmail.com

feed point location, and number of parasitic elements. However, current distribution, radiation pattern, and other characteristics are greatly affected by mutual coupling between elements [18–21].

In this paper a right-angled isosceles triangular microstrip antenna (RITMA) (45°–90°–45°) with inset feed as a basic element is designed first. It is fractured using the Koch fractal technique, and then meander lines are added to it. A planar array of 2 × 2 using this single patch as a basic element is designed for better results in terms of return loss, bandwidth, gain, and directivity. Details of the antenna design are described and simulation and experimental results of return loss, gain, and polar plots of the proposed antenna are presented.

2. Mathematical modeling

The resonance frequency of RITMA structure in TM_{mn} mode is computed using Eq. (1) [22].

$$f_r = \frac{c\sqrt{m^2+n^2}}{2a\sqrt{\varepsilon_r}} \tag{1}$$

Here a is the patch side length, c is the velocity of light in free apace, m and n are mode indices, and ε_r is the reflective index of the substrate material.

The effect of fringe fields is incorporated in the present analysis by replacing the dimension of the patch by effective side length a_{eff} in Eq. (1) as:

$$a_{eff} = a(1+q), \tag{2}$$

where q is evaluated by Eq. (3).

$$q = \left[\frac{h}{a}\left\{0.25\frac{a}{h} + 0.441 + 0.082\left(\frac{\varepsilon_{r,eff}-1}{\varepsilon_{r,eff}^2}\right) + \left(\frac{\varepsilon_{r,eff}-1}{2\varepsilon_{r,eff}}\right)\left(1.451 + \ln\left(0.25\frac{a}{h}+0.94\right)\right)\right\} - 0.25\right]\left(\frac{\varepsilon_{r,eff}+0.3}{\varepsilon_{r,eff}-0.258}\right) \tag{3}$$

Here the effective reflective index of substrate material ($\varepsilon_{r,eff}$) is given by:

$$\varepsilon_{r,eff} = \frac{\varepsilon_r+1}{2} + \frac{\varepsilon_r-1}{4}\left(1+12\frac{h}{a}\right)^{-1/2}. \tag{4}$$

Here h is the height of the substrate. The resonant frequency can then be calculated as follows:

$$f_{m,n} = \frac{c\sqrt{(m^2+n^2)}}{2a_{eff}\sqrt{\varepsilon_{r,eff}}}. \tag{5}$$

The area between the ground and the patch is treated as a cavity bounded by magnetic walls along the edges of the patch and electric walls above and below. The orthogonal edges are identical in length; therefore, the interior modes in the antenna will be TM_{mn} modes to z. The electric field components within the substrate of this linearly polarized aerial are z-directed and the total electric field at the aperture of the aerial is written as the sum of the electric fields associated with modes. The solution of the wave equation for E_Z in the cavity with excitation current in the z-direction is obtained after finding its eigenfunction ψ_m, i.e.

$$\left(\nabla^2 + k^2\right) E_z = j\,\omega\mu_o J_z. \tag{6}$$

Here $\omega$is angular frequency, μ_o is permeability in free space, and J_z is excitation surface current density. k(wave number of the dielectric material) is given by the following:

$$k = k_o \sqrt{\varepsilon_r(1 - j \tan\delta)}. \tag{7}$$

Here $tan\ \delta$is the loss tangent of the material.

The z-directed components of the electric field in the cavity of the patch reduces as shown in Eq. 8 [23,24].

$$E_Z = E_0 \cos\left(\frac{m\pi x}{a}\right) \cos\left(\frac{n\pi y}{a}\right) \tag{8}$$

E_o is the electric field constant. Scaling, copying, and translation of the subarray are done to produce the fractal array. The total field (E_T) of the array implies the field of a single element, which is placed at the origin, increased by a factor; this factor is known as the array factor. To implement directive radiation patterns, it is crucial that the fields from the components of the array add in the desired directions and cancel each other in the remaining area [25–28].

$$E_T = [E(\text{single element at reference point})] \times [\text{array factor}] \tag{9}$$

For a linear array along the x-axis that has M elements, the array factor is given by:

$$AF = \left[\sum_{m=1}^{N} I_{m1} e^{j(m-1)(kd_x \sin\theta \cos\phi + \beta_x)}\right], \tag{10}$$

where sin θ cos ϕ = cos γ is the directional cosine with respect to the x-axis. All elements are at equal intervals, i.e. $d_x$and a dynamic shift β_x.

I_{m1} denotes the magnitude of the element at the point with the following coordinates:

$$x = (m - d)d_x, y = 0. \tag{11}$$

If the number of arrays is N and they are fixed in the y-direction, it gives rise to a rectangular array. The distance between elements is d_y and the phase shift along each row is β_y. The current distribution along the x-directed array is compatible but the complete value corresponds to a part of I_{1n} (n =1,..., N).

Therefore, the array factor for the entire array is given by the equation below.

$$AF = \sum_{n=1}^{N} I_{1n} \left[\sum_{m=1}^{N} I_{m1} e^{j(m-1)(kd_x \sin\theta\ \cos\phi + \beta_x)}\right] e^{j(n-1)\,(kd_y \sin\theta\, cos\phi + \beta_y)} \tag{12}$$

3. Antenna design

The proposed antenna array structure is based on the Koch fractal concept up to the first iteration only; the complexity and the area of the patch are the factors that restricted us for further iterations. The antenna uses a microstrip line feed with inset cut as it provides better matching without any additional matching element. The configuration of the Koch fractal antenna array is shown in Figure 1. It uses the Rogers RT5880-lossy (ϕ_r = 2.2) as a substrate that has a height of 2.5 mm. For an electrically thin ($h << \lambda_0$) RITMA structure having the TM_{10} mode for the antenna, the right isosceles triangle microstrip patch has a length of 4.4 cm, hypotenuse of 6 cm, and resonance frequency f_r = 2.402 GHz, calculated using Eq. (1).

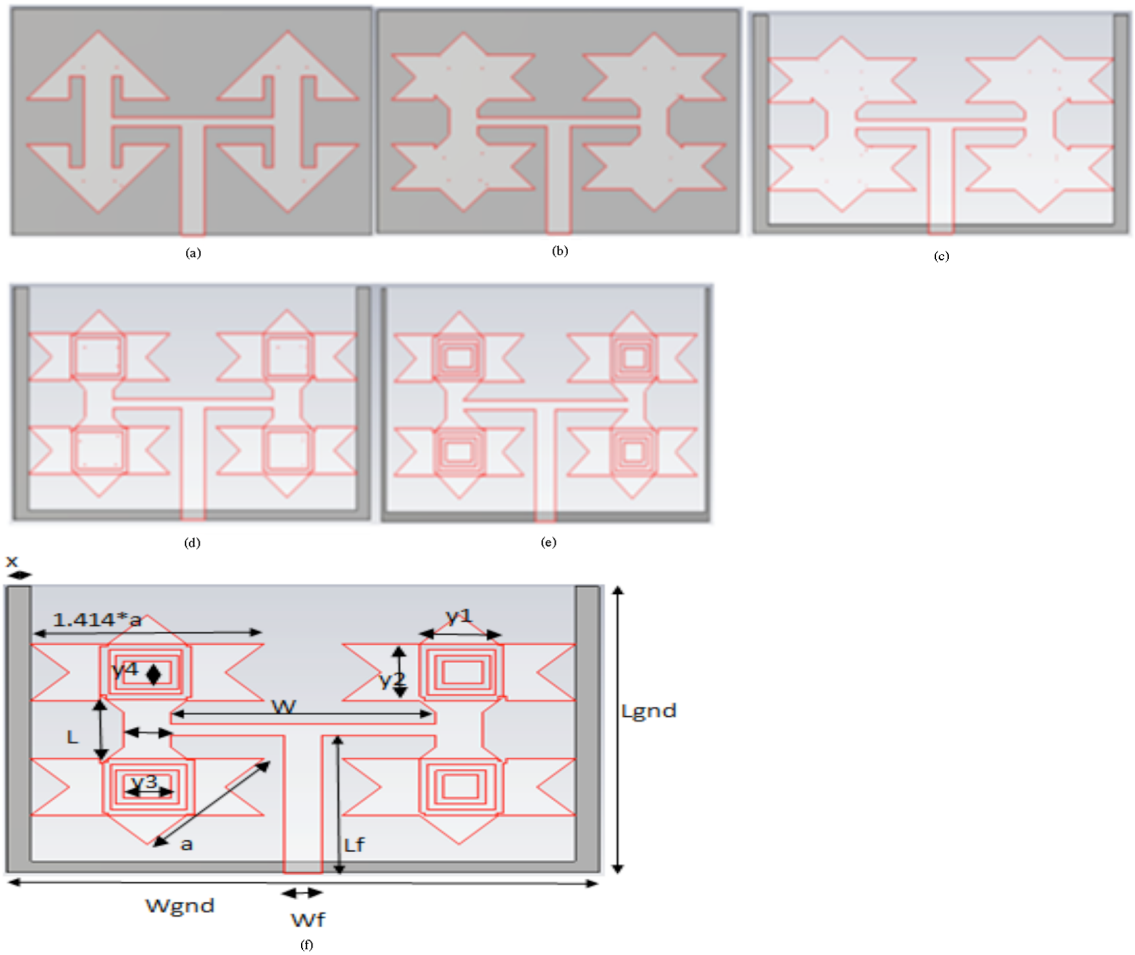

Figure 1. a) Planar array using right isosceles triangle microstrip antenna, b) fractured array, c) defected ground structure, d) structure using single meander lines, e) structure of array using double meander lines, f) geometry of array structure.

The patch has a feed line of width $W_f = 2.5$ cm and length $L_f = 5$ cm, which is obtained by impedance matching of 50 Ω, and on the other side the ground plane has width $W_{gnd} = 7.6$ cm and length $L_{gnd} = 4.4$ cm, which is calculated after placing the array. A simple triangular patch array with inset feed and fractal shape does not give good results in terms of return loss, bandwidth, and gain. Matching needs to be achieved between the patch and feed line over an extensive frequency range for better results. This matching is achieved by clipping the ground plane. The inductive attribute of the patch is balanced by the capacitive load that arises by clipping the ground plane and finally pure resistive input impedance persists. Bandwidth and return loss levels are controlled by this clipping by adjustment in the capacitance that arises between the patch and the ground. Since the results were not satisfactory, we added meander line technology to further improve the return loss, which reduces the size of the antenna and allows wideband operation.

For the purpose of reducing the size of the transponder, a meander-line antenna is an attractive choice. This class of antennas provides the largest size reduction at a given frequency. In this design the outer horizontal meander line has a length of y1, the vertical meander line has length y2, the inner meander line has horizontal length y3 and vertical length y4, and the widths of meander lines are x1. These dimensions are decided based on the Koch fractal structure. The inner edges of the star shape are connected through it. The distance between

the meander lines is 0.5 cm. The number of meander lines is limited as it increases the complexity of the structure.

4. Results and discussion

The designing of the array is the same as for a single patch and they all have the same parameters. We have coupled them in a plane by series and parallel coupling for enhancing the overall performance of the antenna because researches have proved that besides a single patch, an array has advantages like a wide band, increased gain, and bandwidth. The fabricated antenna array is shown in Figure 2.

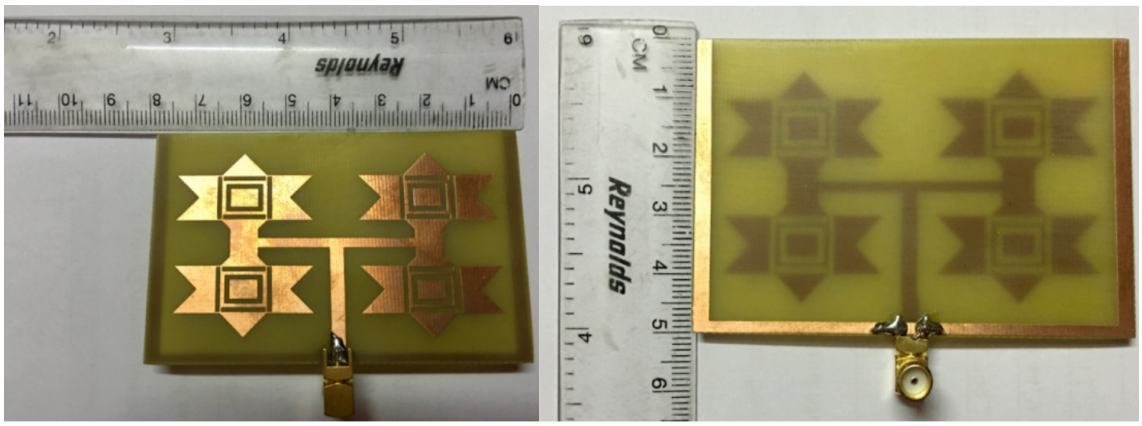

Figure 2. Prototype fabricated antenna.

At the first stage in the proposed antenna design the width of the feed was varied (W_f) as shown in Figure 3 and results were observed. By adopting a series-parallel feed technique, impedance bandwidth of 1.40 GHz is observed and circular polarization of the antenna array is greatly improved. The loss of the feed line is also reduced, and gain of the array as high as 9.60 dB is achieved correspondingly. The feed network consists of several two-way power dividers, which are designed to produce an impedance match at the array input. These variations in feed width are observed by keeping other parameters constant. The return loss (S_{11}) graph with different values of W_f is observed over the frequency range of 1–11 GHz. The width of the feed decides the power distribution of the antenna. However, it cannot be increased beyond a certain limit as it increases the coupling effect. Here in this case the width is varied from 1.5 to 3 cm. It has been observed that keeping the width at 2.5 cm gives optimum results.

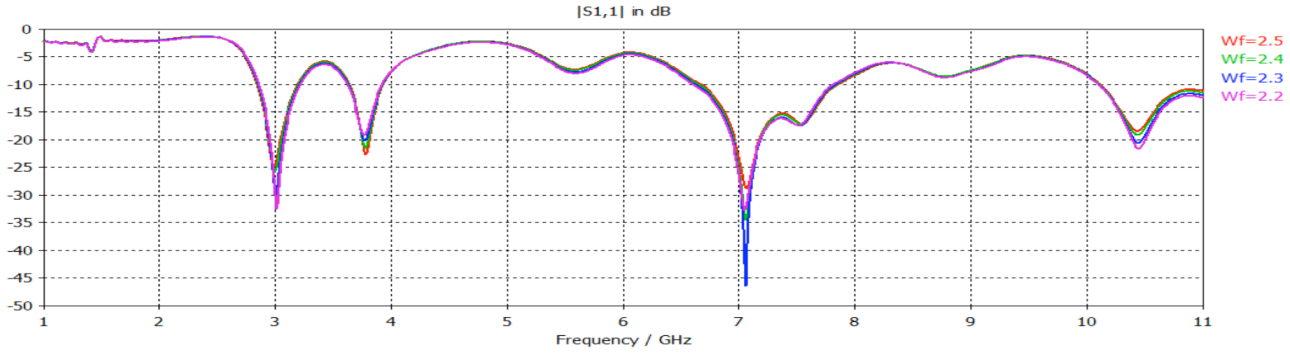

Figure 3. Comparison of return loss with variation in W_f.

In the second stage, the feed width of the single patch (W_{if}) is varied and results are shown in Figure 4 keeping the width of the feed constant. Again an inset fed feeding technique is chosen for individual patches because the input impedance of the antenna can be easily controlled by varying the feed length and width of the inset feed. Return loss improves when proper matching is done. By varying the width of the inset feed, we found that 0.6 cm gives optimum results.

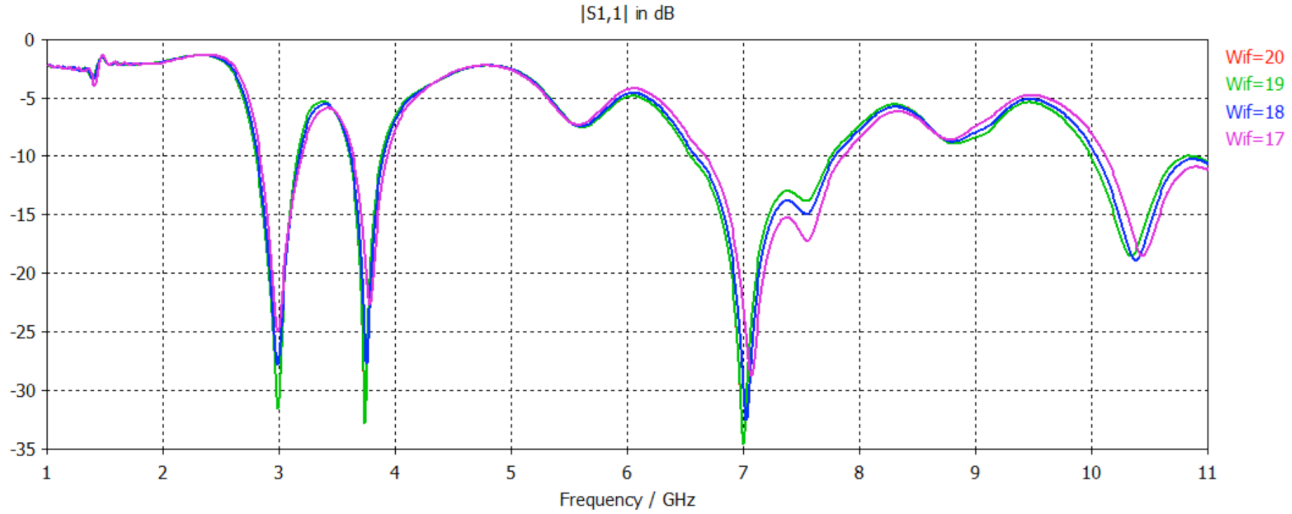

Figure 4. Comparison of return loss with variation in W_{if}.

The equivalent diagram of the defected ground structure (DGS) is shown in Figure 5. The equivalent diagram shows L and C parameters; however, there is no direct relation between dimensions of the DGS and values of passive components. The derived performance of the DGS is not fully predictable until the optimized solutions are achieved through a trial-and-error iterative process. Hence, the conventional methods reported in the literature [14,15] are time-consuming and may not lead to optimum design. The impedance bandwidth could be further enhanced by applying different sizes of ground plane lengths. For this, variations in ground dimensions (x) were done as shown in Figure 6.

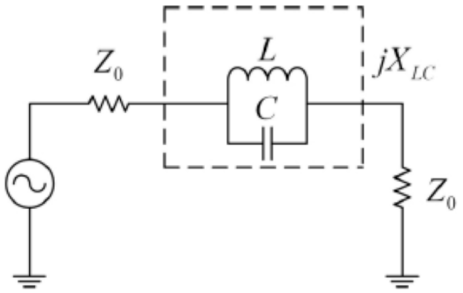

Figure 5. Equivalent diagram of DGS.

Further bandwidth and matching improvements can be obtained by adding meander lines. Group delay and phase plot are shown in Figures 7 and 8, respectively. Nearly linear characteristics are observed for the proposed antenna.

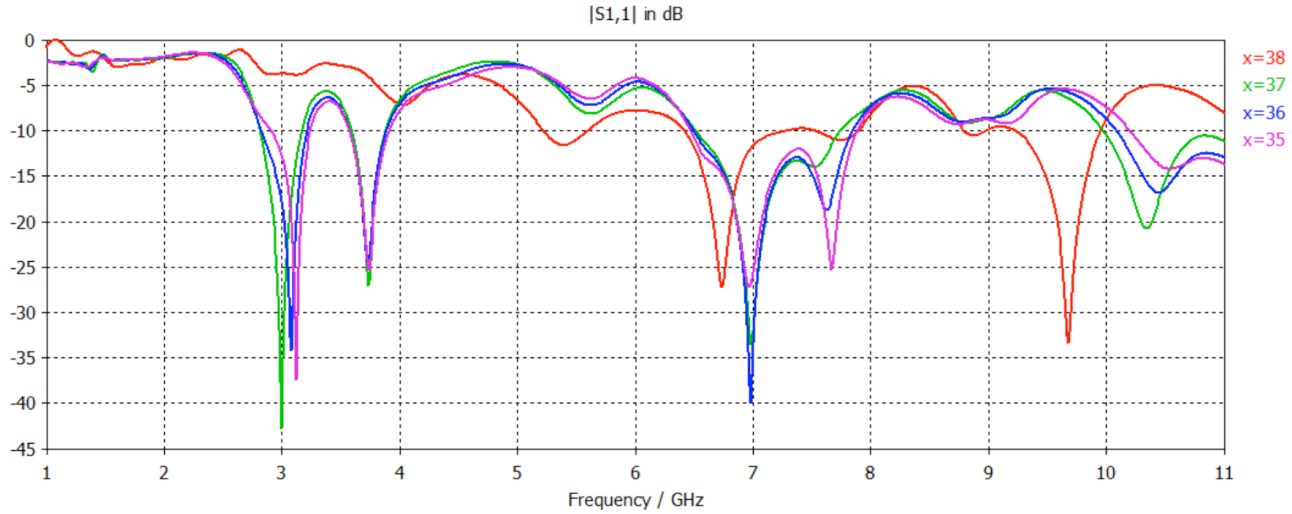

Figure 6. Comparison of return loss with variations in defected ground structure (x).

The flow chart of design steps is shown in Figure 9.

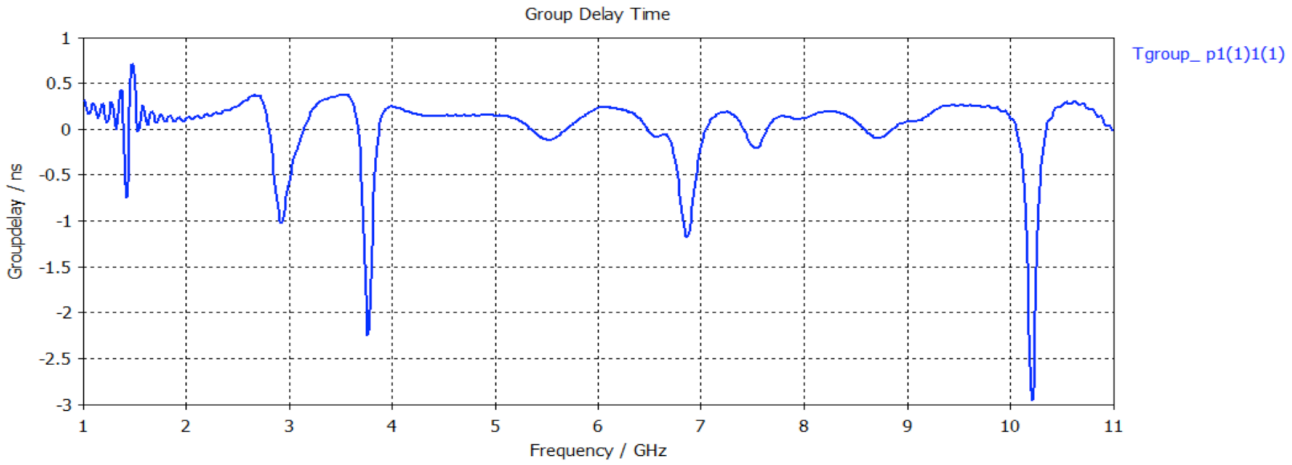

Figure 7. Group delay for the array structure.

Table 1 shows the summary of characteristics of different structures. We can obtain a detailed analysis of the array with meander lines from Table 1, which shows multiband behavior with better gain as compared to arrays without having meander lines. The 3D radiation pattern is shown in Figure 10 at different resonant frequencies. Figure 11 shows a graph between gain vs. frequency.

The return loss, resonance frequency, and input impedance measurements are carried out by using Vector Network Analyzer and its associated computer programs. During impedance measurements, due consideration was given to the accuracy enhancement technique to correct directivity, effective source matching, and frequency tracking errors. The measured resonance frequency of the array antenna using the network analyzer was found at around 2.9 GHz, 3.7 GHz, 6.9 GHz, and 10.35 GHz. The measured return loss and Smith chart for the designed antenna are shown in Figures 12 and 13, respectively.

Figure 14 shows the polar plot patterns at resonant frequencies. These patterns are measured by placing the antenna structure inside an anechoic chamber. The test antenna is mounted on an arrangement lying on a

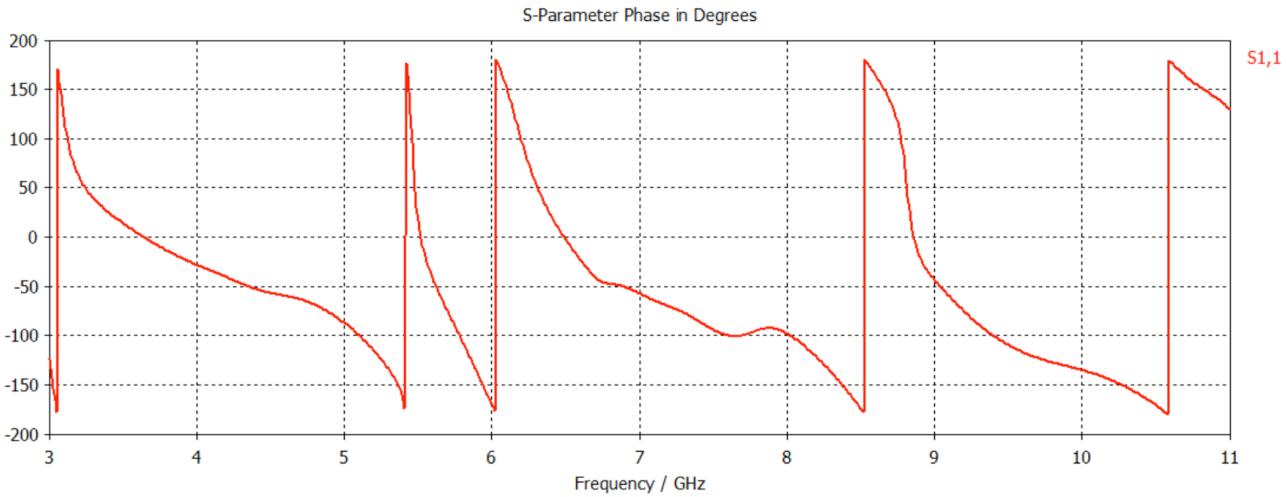

Figure 8. Phase of the reflection coefficient vs. frequency of the antenna.

Table 1. Summary of characteristics of different structures.

Types of structures	Return loss (dB)	Bandwidth (MHz)	Gain (dB)	Directivity (dBi)	VSWR
Planar array (dual band)	−12.08 (5.87) −15.82 (9.44)	130.9, 469.6	10.37, 7.20	10.29, 7.00	1.68, 1.42
Planar array with fractal (dual band)	−24.98 (8.1) −16.21 (10.11)	159.4, 542	8.21, 8.20	8.21, 8.04	1.49, 1.55
Planar array with fractal and DGS (multiband)	−20.81 (2.77) −21.34 (7.40) −14.18 (10.63)	110.4, 730, 708	4.76, 6.33, 9.60	5.66, 6.04, 9.47	1.30, 1.21, 1.46
Planar array with fractal and DGS and single meander line (multiband)	−13.95 (3.1) −23.65 (3.65) −20.31 (7.0) −22.16 (7.8) −15.36 (10.45)	274.7, 337.3, 872.4, 651.5, 801	5.11, 3.58, 6.1, 5.67, 8.24	5.39, 3.52, 5.84, 5.34, 8.11	1.51, 1.15, 1.21, 1.17, 1.40
Planar array with fractal and DGS and double meander lines (multiband)	−36.77 (3.1) −24.83 (3.7) −26.63 (6.9) −24.95 (7.6) −14.20 (10.55)	329.9, 329, 1.40, 799.23	4.58, 4.20, 6.16, 4.85, 9.82	4.78, 3.72, 5.87, 4.53, 9.65	1.07, 1.13, 1.09, 1.12, 1.48

circular wooden platform of 1 m in diameter. With the help of a sweep generator, frequency signals of 2.9 GHz, 3.7 GHz, 6.9 GHz, and 10.35 GHz are applied and radiation patterns are measured by changing angle θ from 0° to 360°. Table 3 shows the comparison between measured and simulated results.

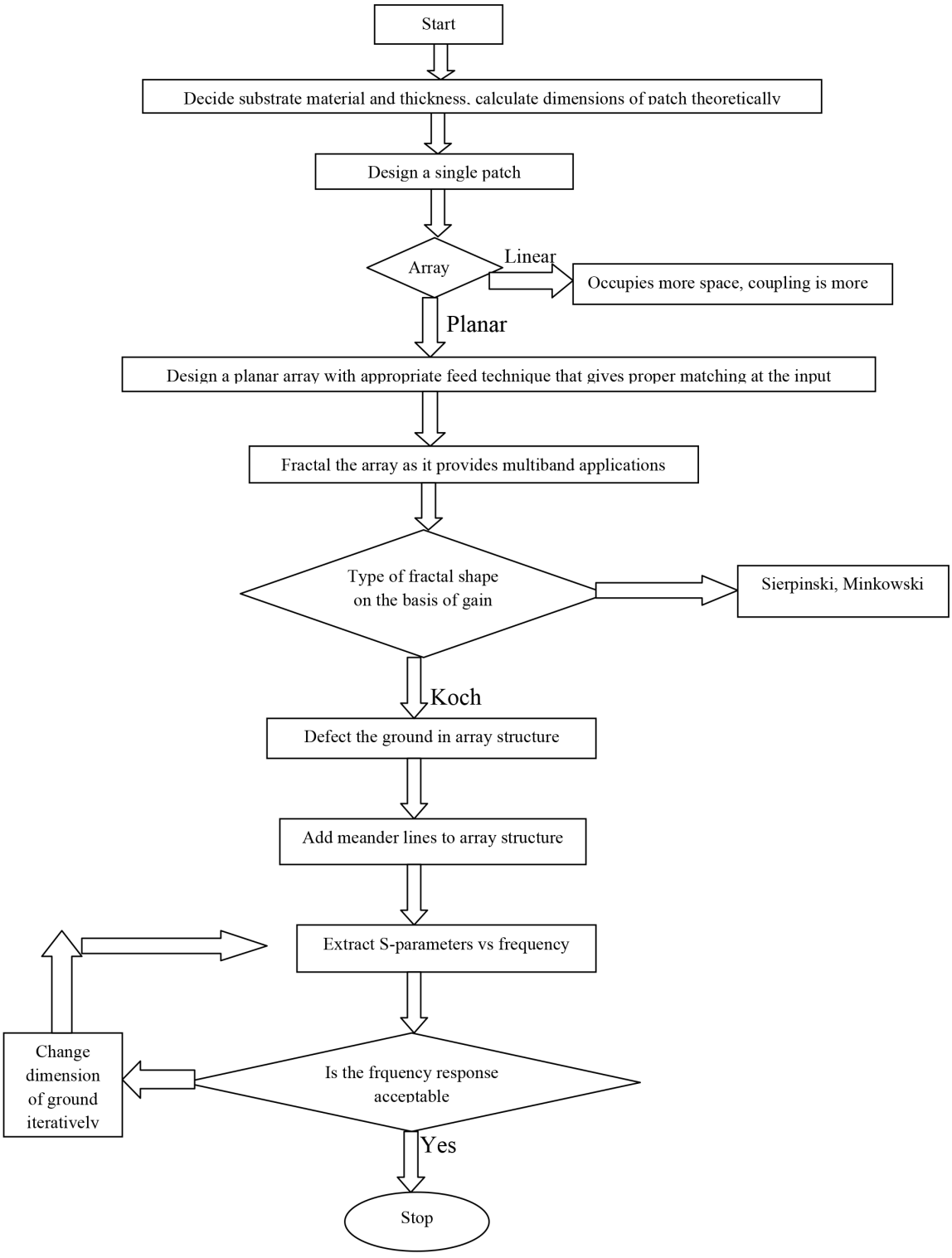

Figure 9. Flowchart for design steps.

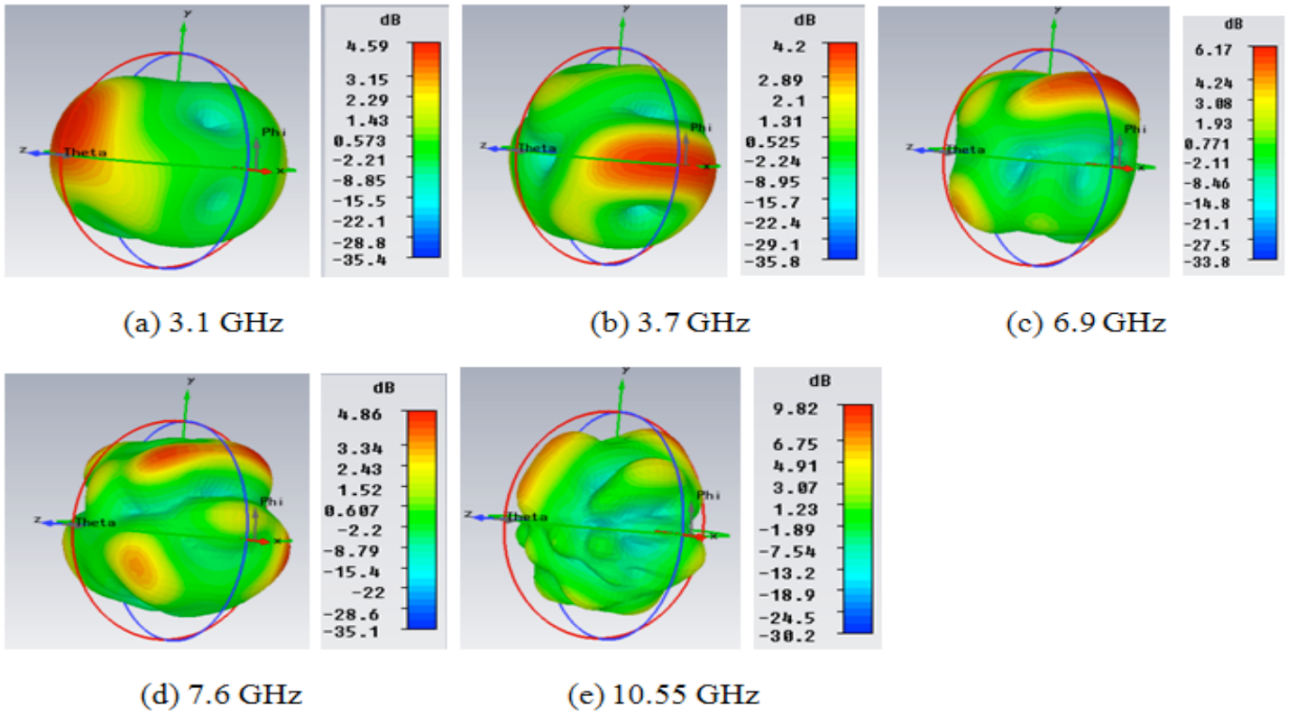

Figure 10. Radiation pattern of array structure.

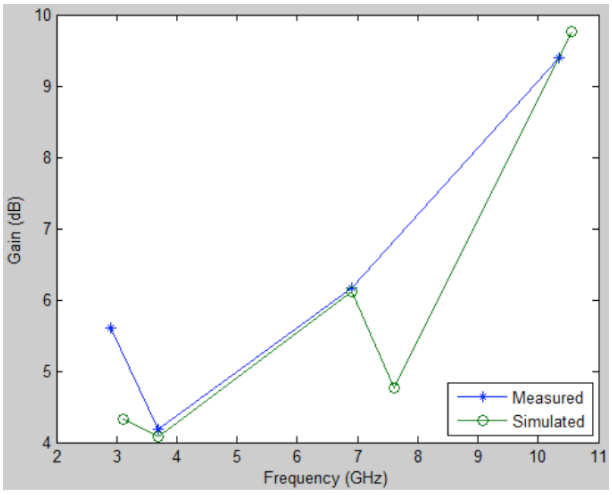

Figure 11. Antenna gain vs. frequency.

Table 2. RITMA array with meander lines and notch ($\phi = 90°$).

Resonant frequency (GHz)	Side lobe level	Angular width (3 dB)	Main lobe magnitude (dB)	E-field (dBv/m)	H-field
3.1	Null	100	4.6	19.31	–32.21
3.7	Null	52.8	4.2	18.90	–32.62
6.9	Null	32.9	5.6	20.87	–30.65
7.6	Null	44.7	3.2	19.51	–32.01
10.55	Null	36.7	9.8	24.37	–27.16

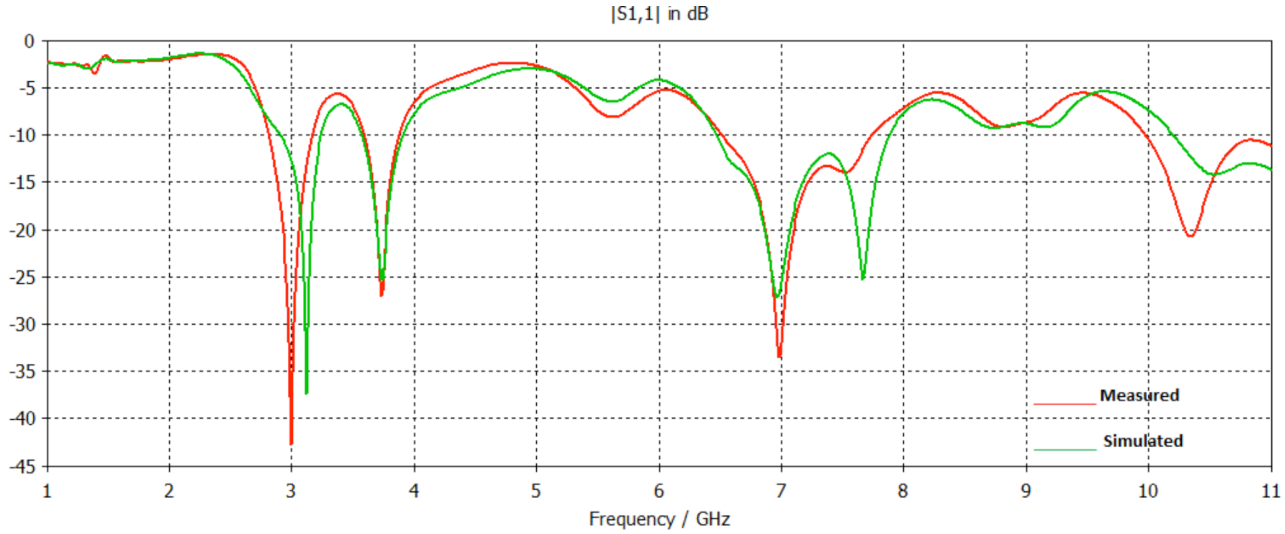

Figure 12. Return loss comparison between simulated and measured results.

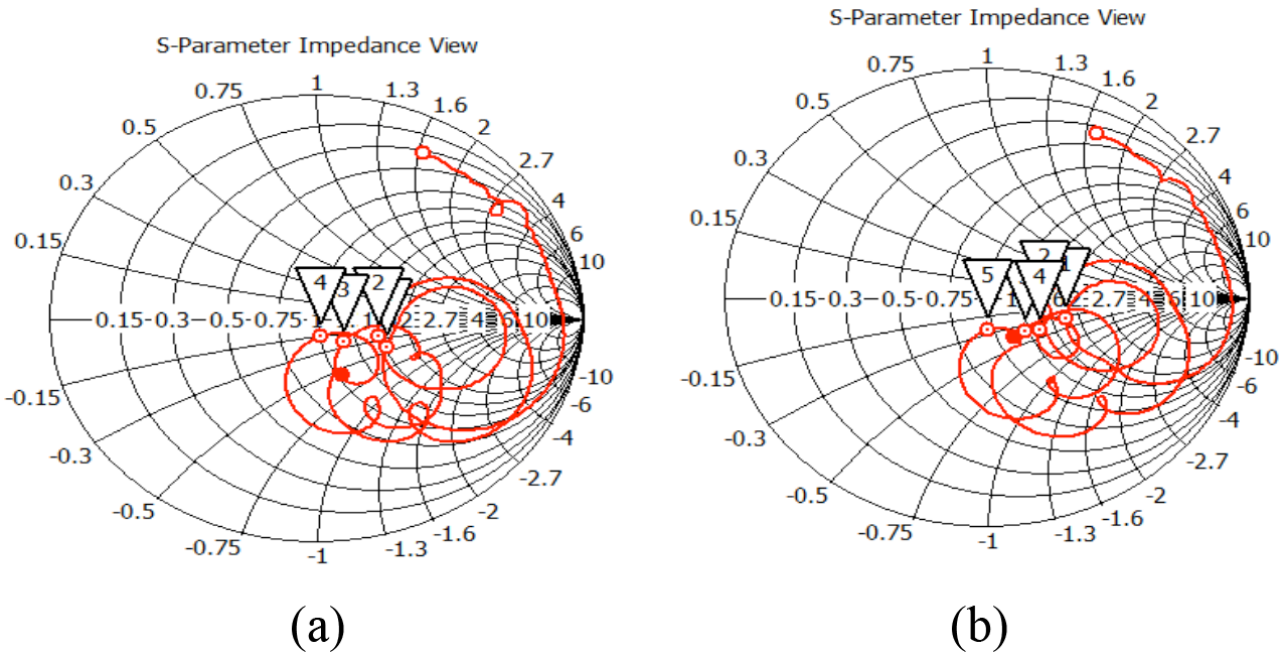

Figure 13. Smith chart: a) measured, b) simulated.

Table 3. Comparison between simulated and measured results of array.

Parameters	Simulated	Measured
Resonant frequency (GHz)	3.1, 3.7, 6.9, 7.6, 10.55	2.9, 3.7, 6.9, 10.35
Bandwidth	329.9, 329, 1.40, 799.23	358, 276.3, 1.22, 870.5
Directivity (dBi)	4.78, 3.72, 5.87, 4.44, 9.60	6.12, 3.82, 5.92, 9.28
VSWR	1.07, 1.13, 1.09, 1.12, 1.48	1.08, 1.14, 1.08, 1.20

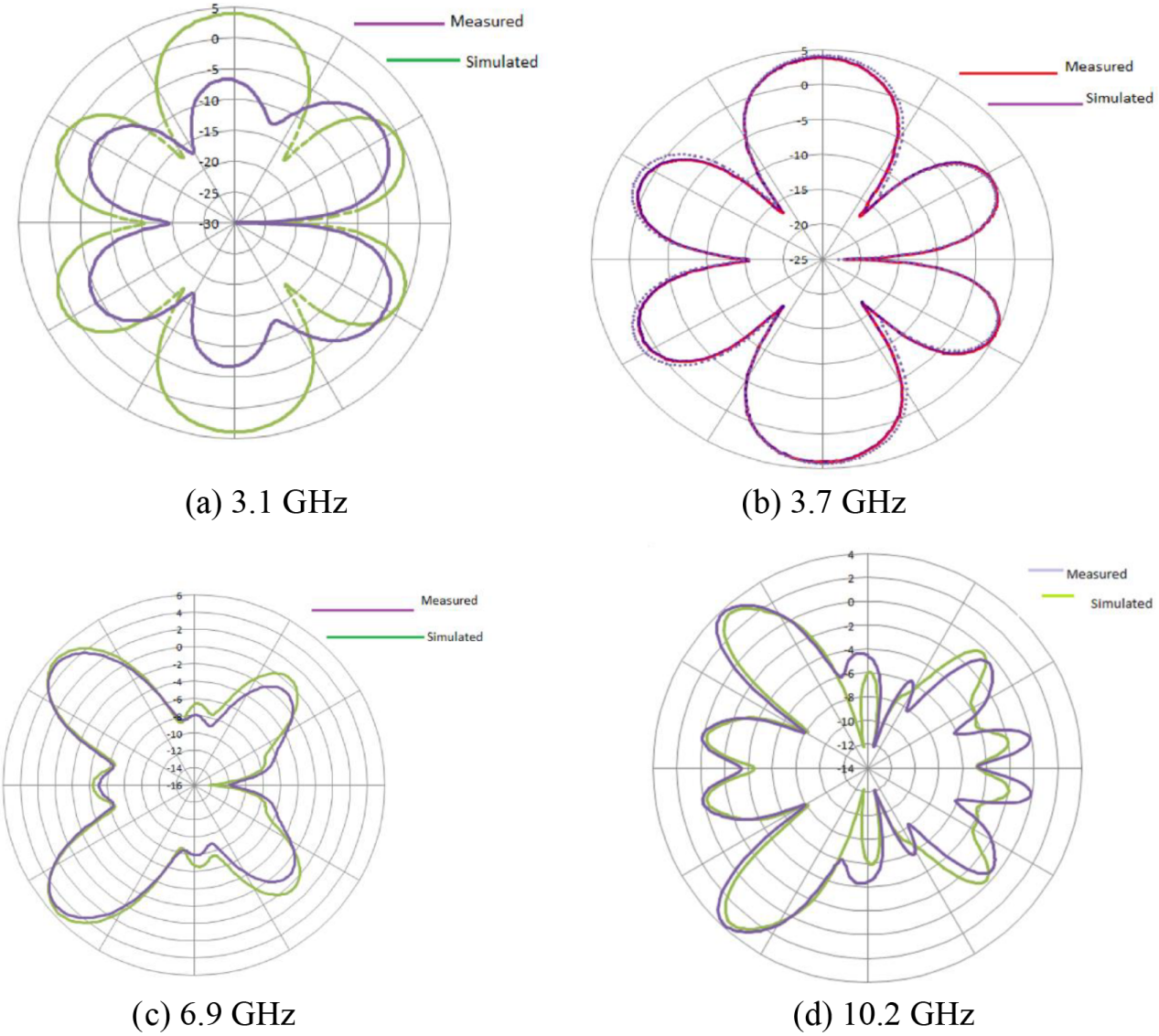

Figure 14. Measured and simulated polar plots for different resonant frequencies.

5. Conclusion

A RITMA planar array has been designed and successfully implemented that gives better results than a single element but shows a single band. By fracturing the antenna bands increase but gain decreases so various methods have been introduced to increase the gain. Utilizing meandered connecting lines, the equivalent inductance between electronic band gap elements is significantly increased. Therefore, reduced size and a wider band gap frequency are obtained as compared to conventional antennas. Increasing the turns in meander lines moves the resonant frequency lower and helps in achieving better impedance matching. The meandered slot position and dimensions are optimized to achieve band-notched behavior. At higher resonant frequency the distribution of surface current is varied around the slot. The measurement results are in good agreement with the simulated data.

Acknowledgment

The authors would like to thank Professor Deepak Bhatnagar, University of Rajasthan, Jaipur, for providing us with the measurement facilities in the lab.

References

[1] Islam MT, Cho M, Samsuzzaman M, Kibria S. Compact antenna for small satellite applications. IEEE Antenn Propag M 2015; 57: 30-36.

[2] Ko SCK, Murch RD. Compact integrated diversity antenna for wireless communications. IEEE T Antenn Propag 2001; 49: 954-960.

[3] Kaka AO, Toycan M. Modified hexagonal Sierpinski gasket-based antenna design with multiband and miniaturized characteristics for UWB wireless communication. Turk J Electr Eng Co 2016; 24: 464-473.

[4] Sondaş A, Uçar MHB, Erdemli YE. Tunable SRR-based substrate for a microstrip patch antenna. Turk J Electr Eng Co 2012; 20: 159-168.

[5] Elsheakh DN, Elsadek HA, Abdallah EA, Elhenawy H, Iskander MF. Enhancement of microstrip monopole antenna bandwidth by using EBG structures. IEEE Antenn Wirel Pr 2009; 8: 959-962.

[6] Shah SIH, Bashir S, Altaf A, Shah SDH. Compact multiband Microstrip patch antenna using defected ground structure. In: IEEE 2014 Direct and Inverse Problems of Electromagnetic and Acoustic Wave Theory Conference; 6–11 September 2014; The Hague, Netherlands. New York, NY, USA: IEEE. pp. 2367-2370.

[7] Bala BD, Rahim MKA, Murad NA. Bandwidth enhanced microstrip patch antenna using metamaterials. In: IEEE 2012 Applied Electromagnetics Conference; 12–13 December 2012; Melaka, Malaysia. New York, NY, USA: IEEE. pp. 280-282.

[8] Anguera J, Ortigosa EM, Puente C, Borja C, Soler J. Broadside triple-frequency microstrip patch radiator combining a dual-band modified Sierpinski fractal and a monoband antenna. IEEE T Antenn Propag 2006; 54: 3367-3373.

[9] Biswas S, Guha D, Kumar C. Control of higher harmonics and their radiation in microstrip antennas using compact defected ground structures IEEE T Antenn Propag 2013; 61: 3349-3354.

[10] Vemagiri J, Balachandran M, Agarwal M, Varahramyan K. Development of compact half-Sierpinski fractal antenna for RFID applications. IEEE Elect Lett 2007; 43: 1-2.

[11] Werner DH, Ganguly S. An overview of fractal antennas engineering research. IEEE Antenn Propag M 2003; 45: 38-56.

[12] Best SR. On the resonant properties of the Koch fractal and other wire monopole antennas. IEEE Antenn Wirel Pr 2002; 1: 74-76.

[13] Hafezifard R, Moghadasi MN, Mohassel JR, Sadeghzadeh RA. Mutual coupling reduction for two closely spaced meander line antennas using metamaterial substrate. IEEE Antenn Wirel Pr 2016; 15: 40-43.

[14] Guha D, Biswas S, Kumar C. Annular ring shaped DGS to reduce mutual coupling between two microstrip patches. In: IEEE 2009 Applied Electromagnetics Conference; 14–16 December 2009; Kolkata, India. New York, NY, USA: IEEE. pp. 1-3.

[15] Zulkifli FY, Lomorti ST, Rahardjo ET. Improved design of triangular patch linear array microstrip antenna using isosceles-triangular defected ground structure. In: IEEE 2007 Asia Pacific Microwave Conference; 11–14 December 2007; Bangkok, Thailand. New York, NY, USA: IEEE. pp. 1-4.

[16] Gregory MD, Petko JS, Spence TG, Werner DH. Nature-inspired design techniques for ultra-wideband aperiodic antenna arrays. IEEE Antenn Propag M 2010; 52: 28-45.

[17] Subbulakshmi P, Rajkumar R. Design and characterization of corporate feed rectangular Microstrip patch array antenna. In: IEEE 2013 Emerging Trends in Computing, Communication and Nanotechnology Conference; 25–26 March 2013; Tirunelveli, India. New York, NY, USA: IEEE. pp. 547-552.

[18] Çakır G, Sevgi L. Design, simulation and tests of a low-cost Microstrip patch antenna arrays for wireless communication. Turk J Electr Eng Co 2005; 13: 93-103.

[19] Werner DH, Haupt RL, Werner PL. Fractal antenna engineering: the theory and design of fractal antenna arrays. IEEE Antenn Propag M 1999; 41: 37-59.

[20] Siakavara K. Novel fractal antenna arrays for satellite networks: circular ring Sierpinski carpet arrays optimized by genetic algorithms. Prog Electromagn Res 2010; 103: 115-138.

[21] King DD, Peters HJ. Mode theory approach to arrays. IEEE Antenn Wirel Propag Lett 1965; 6: 321-322.

[22] Gupta M, Mathur V. Analysis of right angled isosceles triangular Microstrip patch antenna (RITMA) for UWB applications. IEICE Commun Expr 2016; 5: 13-18.

[23] Tiwari VK, Bhatnagar D, Saini JS, Kumar P. Investigation of radiation properties of a right isosceles triangular microstrip antenna. Indian J Radio Space 2005; 34: 353-356.

[24] Lo YT, Solomon D, Richards WF. Theory and experiment on microstrip antennas. IEEE T Antenn Propag 1979; 27: 137-145.

[25] Bhal IJ, Bharti P. Microstrip Antennas. 2nd ed. Norwood, MA, USA: Artech House, 1980.

[26] Balanis CA. Antenna Theory Analysis and Design. New York, NY, USA: John Wiley, 2005.

[27] Sadiku MNO. Principles of Electromagnetics. 3rd ed. New York, NY, USA: Oxford University Press, 2007.

[28] Nashaat D, Elsadek HA, Abdallah EA, Iskander MF, Hennawy HMEl. Ultra wide bandwidth 2 $\times$ 2 microstrip patch array antenna using electromagnetic band-gap structure. IEEE T Antenn Propag 2011; 59: 1528-1534.